European Congress on Computational Methods in Applied Sciences and Engineering
ECCOMAS 2004
P. Neittaanmäki, T. Rossi, K. Majava, and O. Pironneau (eds.)
V. Capasso and W. Jäger (assoc. eds.)
Jyväskylä, 24–28 July 2004

A FINITE ELEMENT BASED TOOL CHAIN FOR THE PLANNING AND SIMULATION OF MAXILLO-FACIAL SURGERY

Jens G. Schmidt*, Guntram Berti*, Jochen Fingberg*, Junwei Cao* and Gert Wollny† [1]

*C&C Research Laboratories, NEC Europe Ltd.
Rathausallee 10, 53757 Sankt Augustin, Germany
e-mails: {schmidt,berti,fingberg,cao}@ccrl-nece.de, web page: http://www.ccrl-nece.de

† MPI for Human Cognitive and Brain Sciences
Stephanstr. 1a, 04103 Leipzig, Germany
e-mail: wollny@cbs.mpg.de

Key words: Maxillo-facial surgery simulation, finite element method, non-linear elasticity, grid computing

Abstract. *Malformations of the midface can be treated by distraction osteogenesis, i.e. cutting bones and pulling them into the right position. We present a computational toolchain helping to predict the effects of the surgery on the soft tissue displacement. An initial raw CT image is segmented and transformed into a geometric head model, which is used for virtual bone cutting and distracting by the surgeon. Using this input, a 3D volume model is generated and handed over to a remote FEM application, which offers a range of possible material models and discretizations, ranging from simple linear elastic ones to time-dependent, non-linear visco-elastic models; it uses high-performance platforms to perform the distraction simulation. The results are transferred back and can be visualized and interpreted.*

Our work is carried out in the context of a medical Grid computing project which aims at making advanced simulation accessible to the medical practitioner by lowering the technical barriers for the "simulation layman" and by providing transparent and secure access to large remote computational resources.

[1]The work of all authors is supported by the EU under grant IST-2001-37153

1 Introduction

Cleft lip and palate are among the most frequent inborn malformations. A resulting maxillary hypoplasia can be treated by *distraction osteogenesis:* During an operation the appropriate bony part of the midface is separated from the rest of the skull (*osteotomy*) and slowly moved into the ideal position by way of a distraction device (cf. Figure 1). Thus even large displacements over 20 mm can be treated effectively.

Figure 1: Patient before treatment (left) and at end of treatment with distraction device mounted (right). The middle image shows a front view. The cable connects to a data logger device, which records the pulling forces every 6 seconds. It is planned to use this information for validating the nonlinear simulations.

A critical point in this procedure is osteotomy design and predictions of the resulting outcome with respect to aesthetics. Another important question is the optimal adjustment of distraction forces, as on one hand, one wants to pull as fast as possible, while at the other hand, to large stresses cause unnecessary pain for the patient.

In the current clinical practice, planning is solely based on CT scans and the surgeon's experience. Our tool chain allows the surgeon to specify arbitrary cuts of facial bones (pre-processing), to simulate the displacements of bones and soft tissue, and to visualize the results in an appropriate way (post-processing). It therefore provides the possibility to predict and compare the outcome of different surgical treatments *in silico*. Also, by using non-linear simulation approaches, we hope to be able to reliably predict the forces occurring during distraction.

The overall goal of our approach is to give the average clinician access to the advanced simulation technology of such surgical planning tools. Physicians typically lack both technical expertise and time needed to prepare input for numerical simulations. Nor do they generally have access to the necessary HPC (high performance computing) hardware and software.

Thus, a successful approach must provide a specialized toolchain which performs the necessary preprocessing tasks autonomously — except the proper "virtual surgery" — and gives transparent and secure access to remote HPC resources. This work is carried out in the context of the GEMSS project [1], which develops dedicated middleware aimed

at solving these problems. Thus, advanced simulation services are brought closer to the practitioner's desktop.

Related Work

A number of researchers have obtained results in the field of computational maxillo-facial surgery planning. Koch [2] describes a system based on linear elasticity, where osteotomies are specified on 2D pictures. Schutyser et al [3] use a 3D "virtual knife" and emphasize the real-time aspects of simulation, trading accuracy for speed. Zachow et al [4] use a specialized version of the Amira visualization system for most parts of the toolchain, including mesh generation. Simulation is restricted to linear FEM models. Gladilin [5] extends these linear models to first non-linear FEM simulations of the distraction process, using a St.Venant-Kirchhoff material model.

Our approach differs from previous efforts by focussing on autonomous usage by non-technical users, offering transparent access to high-performance platforms, and thus largely eliminating hardware-related constraints. The user can therefore employ compute-intensive, high-fidelity numerical methods (cf. Sec. 3), which are indispensible e.g. for calculating accurate forces.

This paper is organized as follows: In Sec. 2, we give an overview over the components of the toolchain: Sec. 2.2 deals with workflow and Grid-related aspects, Sec. 2.3 points out some image processing problems and their proposed solution, and Sec. 2.4 discusses in some detail the interactive osteotomy tool. Then, we go into the details of the underlying FEM simulation in Section 3, by discussing our physical models as well as our discretization. In order to emphasize the advantages and disadvantages of several element types we show numerical results for a model problem. Finally, we summarize our conclusions and point out further planning in this ongoing research effort.

2 A Toolchain for Virtual Osteotomy

2.1 Introduction

Maxillo-facial surgery planning is a complex task, requiring a number of sub-tasks to be solved. The starting point is typically a computed tomography (CT) image of the patients head. The first step usually is to *segment* this image, that is, to assign material labels to the image voxel (cf. Fig. 4). The segmented image is then transformed into a geometric model of the skull. This model is used for appropriate visualization of the bone structure and to let the surgeon interactively specify bone cuts (osteotomies) and distractions. Using this interactive input, a complete 3D FEM model of the patient's head including cuts and displacement boundary conditions is generated, which is passed to a distraction simulation program. Finally, the output of the simulation is visualized and can be interpreted by the surgeon (Fig. reffig:result).

Most of these steps in general require expert knowledge to be performed well. Now, clinicians typically are not experts in image processing, meshing or FEM simulation. So,

Figure 2: Patient before treatment (left) and simulated surgery (right), using volume rendering of original and deformed CT image

most of the toolchain has to run autonomously (with the obvious exception of the bone cutting task). Furthermore, some of the tasks, most importantly the FEM analysis, but possibly also mesh generation or some image processing components require substantial computing resources which are generally not available at clinics and may be difficult to use (e.g. supercomputers or clusters). Thus, transparent access to remote computing facilities is necessary. On the other hand, some surgeons may already routinely use some third party software, such as volume visualization, for their surgery planning, and may want to incorporate such tools into the toolchain. Also, when improved or new functionalities become available, it is useful to be able to easily replace existing tools or to offer the new tools as an alternative.

These considerations led us to choosing a highly modular approach where the toolchain is composed of loosely coupled components, as opposed to building a monolithic maxillofacial surgery planning application. We now discuss some of the components of such a toolchain and related difficulties. The simulation itself is treated in more depth in section 3. Mesh generation is discussed in [6].

2.2 Workflow management and Grid Computing

We use the Triana workflow editor [7] to manage the toolchain. Triana offers easy workflow configuration via a graphical programming language (Fig. 3 left), and controls workflow execution in a data-driven manner.

We used Triana to wrap remote execution of tools in a transparent way [8] via the GEMSS middleware [9]. The GEMSS middleware, which builds on Web service technology, implements end-to-end security (Fig.3 right), which is paramount in the medical field. The GEMSS system also provides or will provide support for authentification, accounting, performance prediction (Quality-of-Service), and advanced functionality such as service

discovery and negociation.

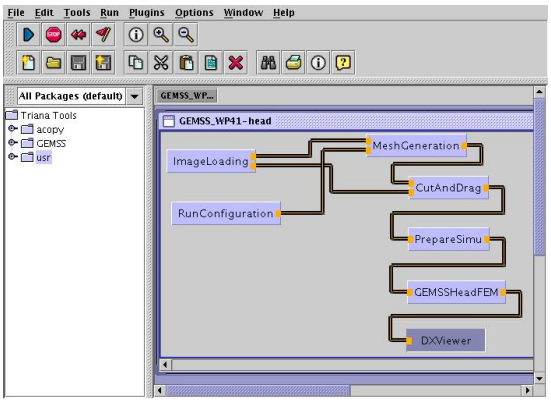

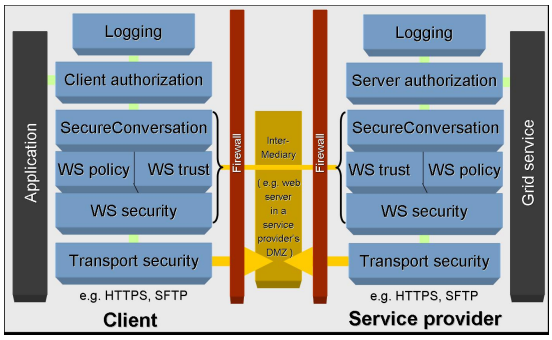

Figure 3: Left: GUI of the Triana workflow manager. A user can easily customize the workflow. Right: Overview of the Web-service based GEMSS security architecture. In contrast to other Grid approachs, GEMSS provides full end-to-end security which is crucial for medical applications.

2.3 Image Processing

Automatic image segmentation is in general an unsolved problem. The more information about the concrete data can be used, the better this problem can be solved. In the concrete case at hand, we use a customized k-means algorithm, which produces useable results.

A problem are metal artifacts e.g. from teeth fillings, which result in spikes in the segmented geometry and may distort the simulation. A number of approaches have been developed for eliminating these beam hardening artifacts [10], most of them operating on the raw CT data before the backprojection. A different problem is possibly missing separation of upper and lower teeth (cf. also the extra cuts needed in Fig. 5). Additionally, soft tissue is difficult to distinguish in CT images.

For these reasons, we also target for a template based segmentation, which we believe can overcome these problems. Based on CT and MRT scans of a healthy individual, a template of the head is in development that includes muscles and fat.

This template head can then be mapped to the individual anatomy by means of non-rigid registration. Here a registration approach is used that combines voxel and landmark information [11]. The landmarks ensure a one-to-one mapping of significant structures especially in the facial area. Hence, image artifacts will no longer yield a false segmentation. The voxel information, on the other hand, drives registration in areas where landmarks cannot be defined properly.

This template based registration will contribute to improved segmentation, in particular reduce effects of metal artifacts and guarantee the proper separation of lower and upper teeth, which is crucial for out biomechanical model. A template registration can

also help to define good default values for a number of auxillary parameters like clipping planes for visualization and simulation.

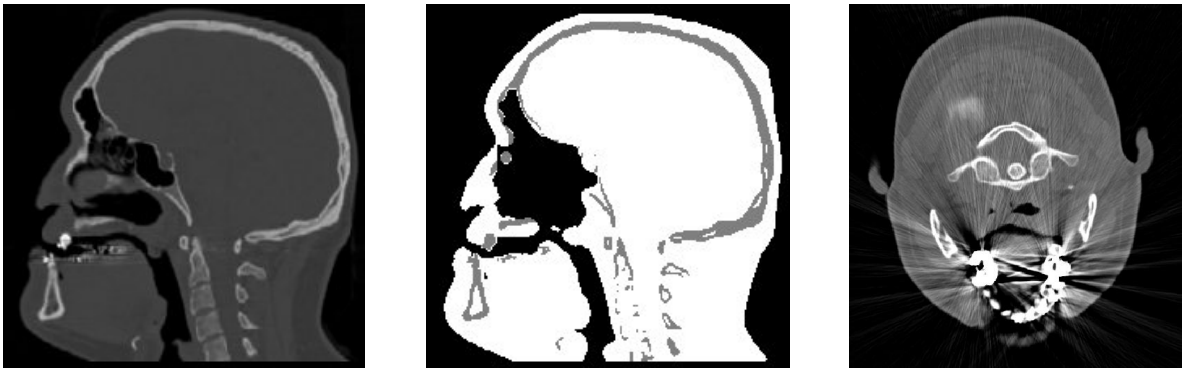

Figure 4: Segmentation using a customized k-means algorithm. Left: Sagittal slice of original CT image. Middle: Segmented slice. Right: An axial slice containing metal artifacts.

2.4 The Virtual Bone Cutting Tool

A crucial step in the toolchain is the specification of bone cuts and displacements. A suitable tool for this task should be sufficiently ergonomic and support the surgeon by giving visual feedback on the actions performed, as well as quantitative information like distances of two points. Ideally, it would be integrated with a cephalometric measurements. Also, there should not be any artificial restrictions e.g. on the number of bone components which can be moved independently.

We chose to build our cutting tool on top of OpenDX [12], because it offers a wide range of visualization features and sufficient interaction capabilities. Also, it is easily extensible by a intuitive graphical programming language and even user-provided modules. Thus, we could quickly arrive at a working prototype by adding a few additional modules.

The flow of action within the cutting tool is as follows: First, the user specifies a number of cuts as closed polygons by selecting points on the bone surface, which is represented by a surface mesh. Then, he chooses bone component(s) to be distracted, and specifies the corresponding translation(s) and rotation(s). An important feedback we plan to integrate in the near future is the visualization of the displacements by moving the components to their specified positions.

After all cuts have been specified, they are converted into three-dimensional volumes which are used to actually apply the cuts on a volumetric model. The conversion takes place in two steps: First, the non-planar polygon is triangulated, and second, this triangulation is extruded using the normal directions at each vertex, with a user-specified thickness.

The complex geometry of the human head may turn the placement of cuts into a tedious problem. In order to support the surgeon, we provide clipping planes and selectable

transparency of the bone. In addition, the 3D location of the cuts is visually emphasized by using balls and tubes for the vertices and edges of the polygons, see Fig. 5.

Another difficulty is the verification of the separation of components. It may happen that parts intended to be separated by cuts are in fact still connected by small bridges, which would grossly distort the subsequent simulation. A possible source of such bridges may be segmentation artifacts such as the missing separation of upper and lower teeth. For finding such bridges, we have developed a coloring tool which colors a component in a wavefront starting from a selected seed point. A bridge will then be detectable as a "color leak" (cf. Fig. 6).

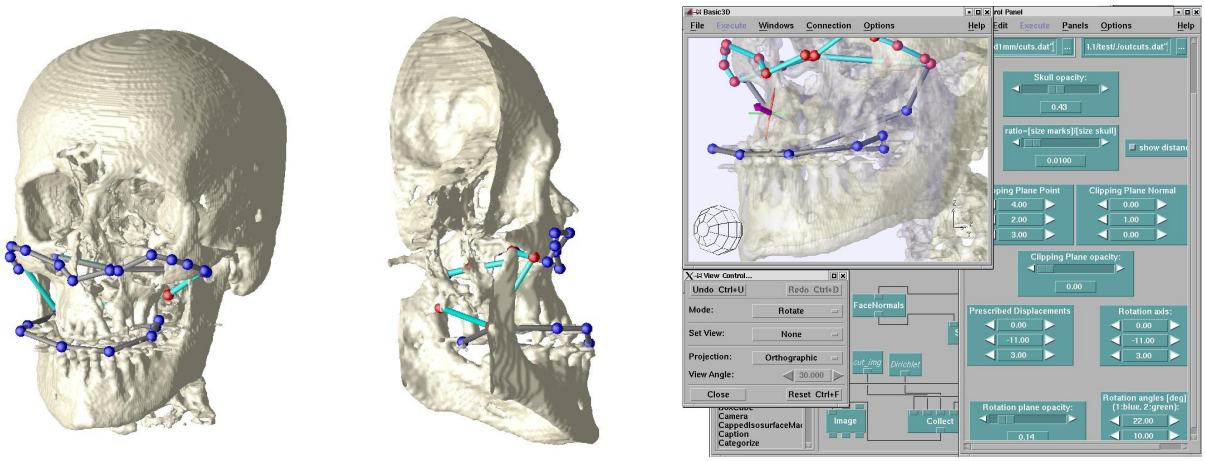

Figure 5: The cutting tool: Front view (left) and side view (middle) with clipping. The current cut is highlighted. The cut separating lower and upper jaw is necessary to overcome segmentation artifacts introducing unphysical connections. Right: Screen shot of the cutting tool.

3 Distraction Simulation

The simulation of the distraction process is done by a Finite Element analysis. Both time and memory requirements of such an analysis are far beyond the capabilities of a single workstation or PC and are therefore carried out remotely on a parallel machine via the GEMSS middleware.

The user can choose between two computation modes. A fast mode that returns a linear approximation of the problem in a few minutes, or a detailed non-linear approximation that can last several hours, and is capable of computing more accurate force distributions, especially in combination with visco-elastic material models. In the next three subsections we will give a brief description of the material laws, the element formulations and the linear solvers we are using.

All computations are carried out on a PC cluster with an AMD Athlon 1900+ CPU and 1 GB of memory at every node. Although scaling is a very important issue for every parallel computation, this topic would be far beyond the scope of this article and is

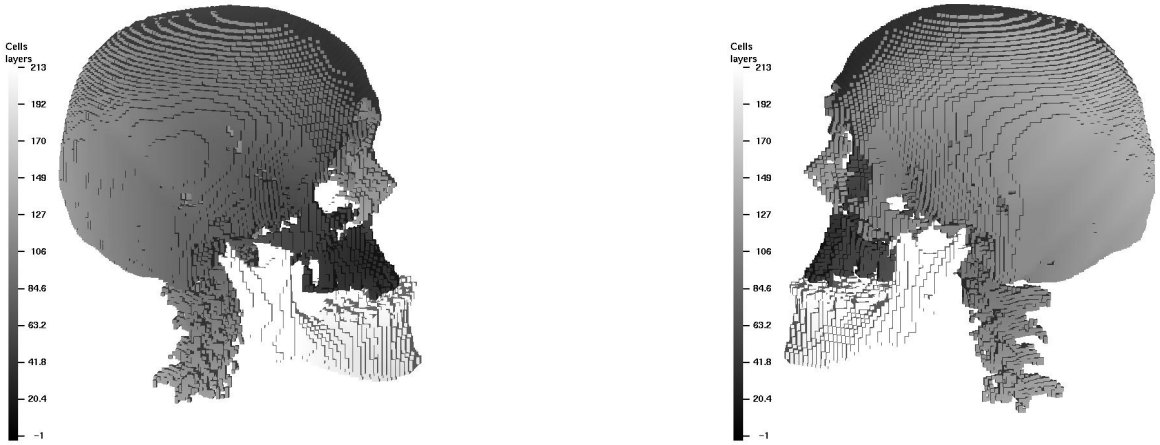

Figure 6: Visualization of bridges by using a wavefront coloring of components. It is clearly visible by the continuous coloring that the maxilla is not entirely cut in the right part (left image). It is also visible that the lower jaw is separated from the rest of the skull.

therefore left out. Since the FEM discretization of the problem is very well suited for parallelization in general, the scaling problem mainly arises in the solver that is used for the linear systems of equations inside the finite element discretization. For the the numerical results shown in this section we used the HYPRE solver library, which is especially written for MPI driven PC clusters and therefore performs and scales very well on the cluster we used, see [13] for more results.

3.1 Physical models and material laws

Our parallel Finite Element code FEBINA uses a fully non-linear model of the distraction process, i.e. we incorporated geometric, material and time dependent nonlinearities in our code. As far as our survey on the recent maxillo-facial simulation softwares shows, this has not been done so far. The following list gives an overview over the three sources of non-linearities and the models we are using.

- The code is build to handle **finite deformations**, i.e. the strains $\mathbf{E}$ are non-linearly depending on the deformations $\mathbf{u}$. The characteristic relation between strains and deformations reads
$$\mathbf{E}(\mathbf{u}) = \frac{1}{2}\left(\nabla\mathbf{u} + \nabla\mathbf{u}^t + \nabla\mathbf{u}^t \cdot \nabla\mathbf{u}\right).$$
- In addition to that the code is based on hyperelastic material laws. From a mathematical point of view a material law is the relation between strains and stresses. A material is called *hyperelastic* if the deformations are independent of the load path, or equivalently, if a stored energy potential W exists, and if the stress-strain relation has the simple form $\mathbf{S}(\mathbf{E}) = \partial W(\mathbf{E})/\partial\mathbf{E}$. Different hyperelastic material laws can

be easily implemented in our code. For our maxillo-facial simulation we use a simple Neo-Hookean material law that reads

$$W(\mathbf{E}) = \mu \left(\mathrm{tr}(\mathbf{E}) - \frac{1}{2} \ln J \right) + \lambda \left(\ln J \right)^2 ,$$

where $J^2 = \det(\mathbf{E} + \mathbf{I})$ holds. Here μ and λ are two material parameters that for small strains coincide with the Lamé parameters of linear elasticity.

- A third source of non-linearity is the timely behavior of the material. Since the deformations shown by a hyperelastic (and therefore elastic) material are independent of the load path, there are

  (a) no permanent deformations without a permanent load and

  (b) no stress free configurations in the presence of permanent deformations.

  But both properties are necessary to describe the behavior of the facial soft tissue for the distraction process we want to simulate. Clearly the material shows property (a) after the treatment. Without this property the head of the patient would deform back to its original position as soon as the pulling process would be ended. On the other hand the desired permanent deformations after the ending of the treatment are not causing permanent stresses in the materials. After a certain amount of time the material does no longer "remember" the pulling process.

  The two properties are called **creep** and **relaxation**. In Figure 7 those properties are briefly sketched. A material that shows creep and relaxation in this way is called a "Maxwell fluid" and belongs to the set of **viscoelastic** materials. Mathematically this type of viscoelastic stresses $\mathbf{S}_v$ are achieved by integrating the time derivative of the stresses over the past and weighting the past stresses by a weight function, which describes how fast the material "forgets" about its past. The material parameter θ_v is a characteristic time period. The most simple viscoelastic time response reads

$$\mathbf{S}_v(\mathbf{E}(t_0)) = \int_{\infty}^{t_0} \frac{\partial W(\mathbf{E}(\tau))}{\partial \mathbf{E}^2} \, \frac{\partial \mathbf{E}}{\partial t} \; e^{-(t_0-\tau)/\theta_v} \; d\tau.$$

For more details on the mentioned non-linearities the reader is referred to [14, 15, 16].

3.2 Discretization and finite element types

The results of the bone cutting tool are used together with the segmented CT-data to create a 3D Finite Element mesh of the skull, details are described in [6]. The resulting unstructured mesh consists of either tetrahedra or hexahedra, and in future version also hybrid meshes consisting of hexahedra, transitional pyramids and tetrahedra will be produced.

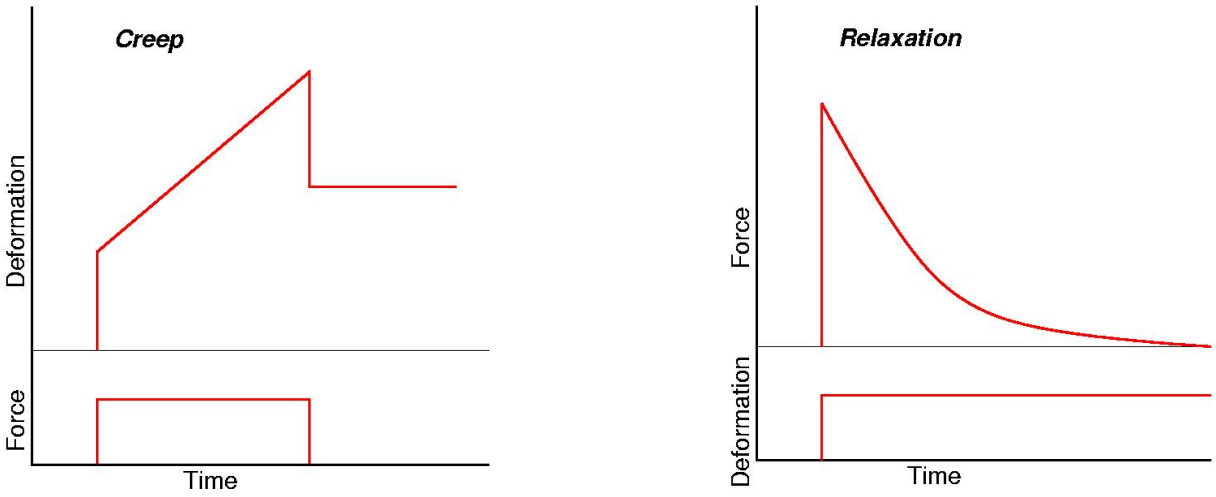

Figure 7: Sketches of viscoelastic creep (left) and viscoelastic relaxation (right) of a Maxwell fluid.

After the discretization of the geometry, we have to choose a finite element formulation to discretize the infinite dimensional solution space. So far the FEBINA code provides the following element types:

T4L Linear form functions for tetrahedra (4 nodes).

T10Q Quadratic form functions for tetrahedra (10 nodes).

H8L Tri-linear form functions for hexahedra (8 nodes)

H20Q Quadratic form function set called "Serendipity" for hexahedra (20 nodes, 3 nodes on every edge, see Figure 8)

EAS Tri-linear form functions for the displacements, and an additional space of enhanced strains of 9,12 or 21 dimensions per element. Since the enhanced strains are discontinous at the element boundaries they are condensed out of the element stiffness matrices localy and do not show up as global unknowns in the matrix. For further details on those elements the reader is referred to [17, 18].

3.2.1 The model problem

In order to test the performance of these element types we designed a simple model problem and meshed it by a regular axis-parallel hexahedral mesh. In order to have a tetrahedral tessalation we divided the hexahedra in five tetrahedras in the standard way without adding new nodes. Table 1 shows the number of nodes and elements for the different mesh sizes.

The reference configuration of the model problem is the axis-parallel brick $[-100, 100] \times [0, 100] \times [0, 100]$ (all length units are mm). This block consists mainly of

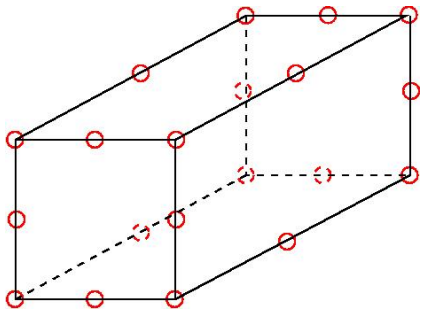

Figure 8: Sketch of the 20 node quadratic hexahedral element H20Q.

	hexahedral meshes		tetrahedral meshes	
relative mesh size	H8L, EAS	H20Q	T4L	T10Q
$h = 1$	625	2,355	4,659	625
$h = 1/2$	4,131	15,363	33,795	4,131
$h = 1/4$	28,611	110,211	257,667	28,611
$h = 1/8$	212,355	833,283	2,012,931	212,355
$h = 1/16$	1,635,075			1,635,075

Table 1: Number of unknowns on different meshes.

a soft material with Young modulus $E = 1\,\mathrm{N/mm^2}$ and a nearly uncompressible Poisson ratio of $\nu = 0.49$. Inside this block of soft tissue there are two blocks modeling the bone. They consist of a hard but compressible material ($E = 1000\,\mathrm{N/mm^2}$, $\nu = 0.25$). These blocks are cubes of length $63.\overline{3}$ mm and their midpoints are at $(\pm 36.\overline{6}, 25, 25)$. Therefore there is only a small gap of 10 mm between them, which is filled with a very soft artificial material ($E = 0.001\,\mathrm{N/mm^2}$, $\nu = 0.25$) in order to model the volume of a cut (see section 2.4), and to avoid penetration problems in a geometrically more complicated real-world case.

The deformation of the model problem is driven by prescribed displacements: One inner blocks is fixed at its bottom surface while the other one is rotated by -20 degrees around the y-axis and translated with the vector $(20, 5, 10)$. Figure 9 shows the resulting position of the blocks inside the soft tissue.

3.2.2 Linear results

For all mesh sizes and all elements mentioned above we carried out a linear computation of the model problem. Figure 10 shows the resulting displacement of the point $(0, 50, 100)$, i.e. the midpoint of the problems bottom plane. This point is of special interest, since for $x = 0$ the soft material is kind of sucked into the widening gap between the blocks and forms a dent on the outside of the soft block. Since the gap between the two blocks has its maximum at the bottom, we choose the bottom point of the block to be measured.

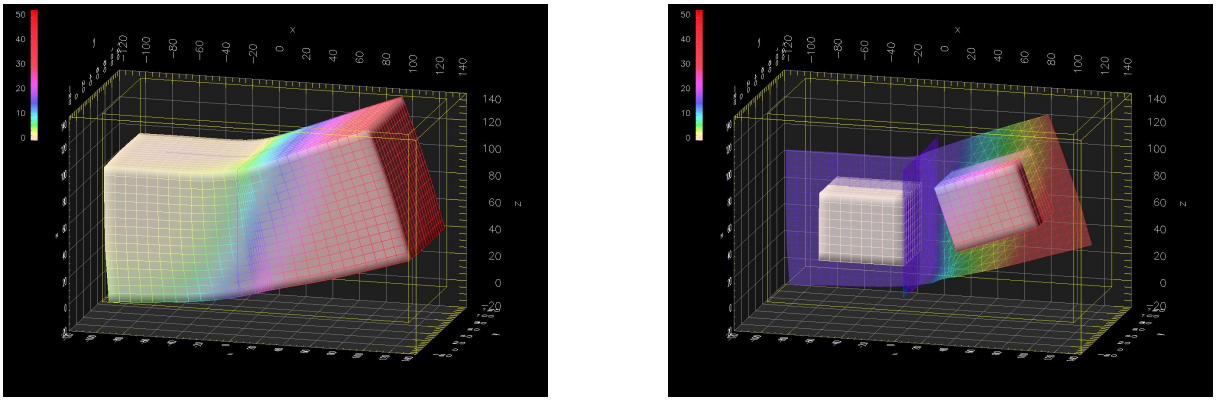

Figure 9: Simple model problem: Two bone-like cubes in a nearly incompressible soft material.

This figure shows the results for our uniform axis-parallel meshes. For distorted meshes, as the one shown in Figure 11, the results look very similar.

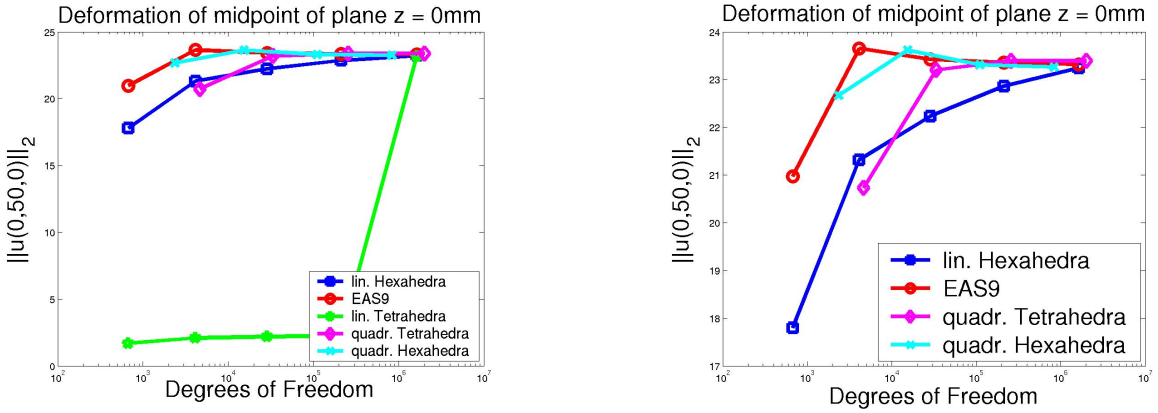

Figure 10: Performance of the different element types on the linearized model problem, with linear tetrahedras (left) and without them.

From these results it is obvious that linear tets are not suited for the approximation of our problems. Among the other elements the EAS9 elements perform best. Even with a comparably small number of elements the solution is very well approximated. This is a well known feature of EAS elements, cf. [17, 19]. The only element that shows comparable results is the quadratic hexahedron H20Q, but this element yield global matrices that have about twice the size of the matrices produced by EAS or H8L elements, since the latter two have about 81 entries in every row for the uniform mesh used in our model problem, whereas the former have 156 entries. Therefore the H20Q element does not only need almost twice the memory, it also leads to higher iteration numbers for the linear solver and therefore to a longer computing time.

For the solution of the linear systems of equations we used the HYPRE solver library, cf. [13]. We choose an iterative solver consisting of a GMRES Krylov subspace solver

	non distorted mesh			distorted mesh		
relative mesh size	H8L	H20Q	EAS9	H8L	H20Q	EAS9
$h = 1$	9	25	12	8	24	12
$h = 1/2$	8	25	12	9	27	13
$h = 1/4$	10	15	13	11	19	13
$h = 1/8$	10	16	12	14	21	15
$h = 1/16$	11		13	17		19

Table 2: Needed iterations of the GMRES(AMG) solver to reach a relative residual of 10^{-6} for different meshes and element types.

preconditioned by HYPRE's Algebraic Multigrid solver BoomerAMG. The linear systems that arise from linearized elasticity are positive definite and therefore a appropriate multigrid solver should show asymptotically optimal iteration numbers, i.e. the iteration number should be independent of the mesh size. As shown in Table 2 this is the case for the axis parallel mesh as well as for distorted meshes. Figure 11 shows one of those distorted meshes.

To sum up our linear experiments one can say that EAS elements in combination with AMG based solvers are a nearly optimal choice for those problems. Using this combination the linear solution process for the large mesh $h = 1/16$ lasts less than 2 minutes on 16 CPUs of the above mentioned cluster. Since the EAS elements yield almost the same accuracy for the mesh of size $h = 1/8$ we can achieve an equally precise result on 8 CPUs in 35 seconds.

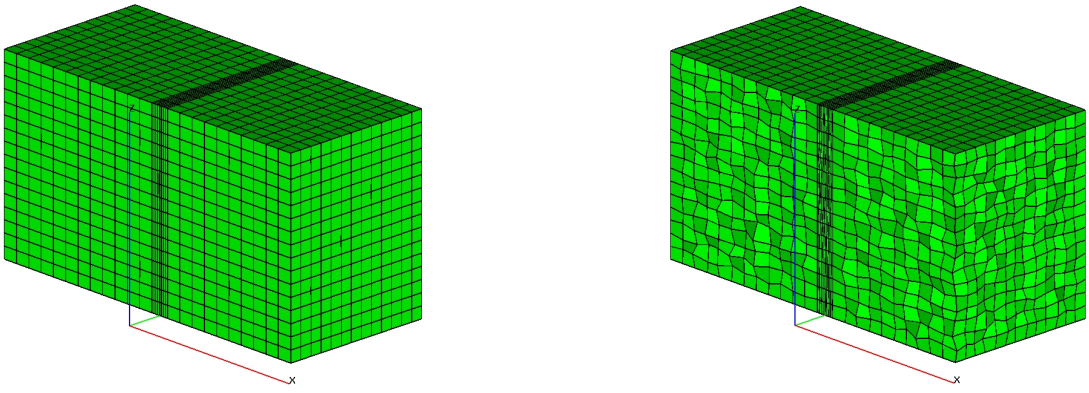

Figure 11: Cut through an undistorted (left) and distorted mesh (right) of relative mesh size $h = 1/4$.

3.2.3 Nonlinear results

In general in the non-linear regime the element types show the same results as in the linear case. But the more successful the elements are in the linear case, the more they lack robustness in the non-linear case. We divided the non-linear computations into ten steps of increasing prescribed deformations, such that the last step reaches the deformations we prescribed in the linear case. During time stepping the elements of the mesh become more and more deformed by the solution of the non-linear process.

The EAS elements can only stand small amounts of distortions. Especially at the points in the mesh around the gap, where elements are massively deformed and the material constants jump by up to 6 orders of magnitude (from $E = 0.001$ to $E = 1000$) those elements cause divergence of the solution process very quickly. This does not come by surprise, since it has been shown in the literature earlier, cf. [19]. One remedy could be the use of advanced stabilized low-order elements, like they are proposed in [20].

Another element type that diverges when the elements become more and more distorted is the quadratic tetrahedra T10Q, although it diverges at a much later time than the EAS elements.

The hexahedral elements seem to be very stable, especially the tri-linear ones.

We also observed that in the case of heavily distorted elements during a non-linear computation there can be small negative eigenvalues found in the spectrum of the system matrix. Therefore the performance of the AMG solver degrades. In our example the iteration number in the last time step of our non-linear model problem increases (compared to the linear case) from 11 to 17 for the H8L elements on the finest mesh and from 16 to 42 for the H20Q element. But this is still an acceptable value.

4 Conclusion

The presented tool chain helps the surgeon predicting the outcome of a distraction osteogenesis for an arbitrary set of cuts and distractions and is expected to be a valuable tool for planning such treatments. By using advanced Grid computing infrastructure, the crucial time and memory intensive parts of the tool chain can be executed remotely on a HPC server. This enables the clinician to get results from adequate state-of-the-art simulation within acceptable times, without needing to worry about technical details or security issues.

The development of the tool chain is still ongoing work. A clinical evaluation of a first is about to start, and feedback from the surgeons will be incorporated. One of the major areas for improvements will be the ergonomy of the virtual osteotomy tool, for example by supporting automatic fitting of cut lines to the skull surface geometry, and to use registration of a template head to import auxiliary data like clipping etc., thus freeing the user from tedious and repitive work.

Another important improvement will concern removal or reduction of metal artifacts which may distort the simulation. We also plan to use the template registration approach

to map more soft tissue details like muscles, and to compare quantitative differences between simulations run with different material laws and resolutions. This will give us a clearer picture of the tradeoffs between computation time, sophistication of material modeling and accuracy of simulation.

The discretization and solver algorithms chosen in our finite element code FEBINA have proven to be well suited for the solution of the numerical problems arising during the simulation of maxillo-facial surgeries. Especially the combination of EAS Elements and AMG solver gives a very fast and quite accurate approximation of the outcome of the surgery. In the future we will try to improve the robustness of the non-linear computations by implementing modern low-order elements. Since the distortion of the elements is the main reason for the problems in the non-linear case, one should consider adaptive remeshing as a possible way to go.

Acknowledgments

The middleware used for the remote execution of the simulation jobs was developed by our partners in the GEMSS project. The image segmentation component was developed by F. Kruggel at the Max-Planck-Institute for Cognitive Neuroscience in Leipzig. We thank Dr. T. Hierl from the University Clinic Leipzig for his kind support and provision of patient data and photographies.

REFERENCES

[1] The GEMSS project: Grid-enabled medical simulation services. `http://www.gemss.de`, 2002. EU IST project IST-2001-37153, 2002–2005.

[2] R.M. Koch. *Methods for Physics Based Facial Surgery Prediction.* PhD thesis, Institute of Scientific Computing, ETH Zürich, 2001, Diss.No.13912.

[3] Filip Schutyser, Johan Van Cleynenbreugel, Joseph Schoenaers, Guy Marchal, and Paul Suetens. A simulation environment for maxillofacial surgery including soft tissue implications. In *Proceedings of MICCAI 1999*, pages 1210–1217, 1999.

[4] Stefan Zachow, Evgeny Gladilin, Hans-Florian Zeilhofer, and Robert Sader. Improved 3D osteotomy planning in cranio-maxillofacial surgery. *Lecture Notes in Computer Science*, 2208:473–481, 2001.

[5] Evgeny Gladilin. *Biomechanical Modeling of Soft Tissue and Facial Expressions for Craniofacial Surgery Planning.* PhD thesis, Fachbereich Mathematik und Informatik, Freie Universität Berlin, 2003.

[6] G. Berti. Image-Based Unstructured 3D Mesh Generation for Medical Applications. In P. Neittaanmäki, T. Rossi, K. Majava, and O. Pironneau, editors, *European Congress on Computational Methods in Applied Sciences and Engineering ECCOMAS 2004*, to appear. Jyväskylä, 24-28 July 2004.

[7] Triana homepage. `http://www.triana.co.uk/`, 2003.

[8] Junwei Cao, Guntram Berti, Jochen Fingberg, and Jens Georg Schmidt. Implementation of grid-enabled medical simulation applications using workflow techniques. In *Proceedings of GCC 2003*, Shanghai, December 7 – 10 2003. to appear.

[9] Siegfried Benkner, Guntram Berti, Gerhard Engelbrecht, Jochen Fingberg, Greg Kohring, Stuart E. Middleton, and Rainer Schmidt. GEMSS: grid infrastructure for medical service provision. In *Proceedings of HealthGrid 2004*, 2004.

[10] K. De Man, J. Nuyts, P. Dupont, G. Marchal, and P. Suetens. An iterative maximum-likelihood polychromatic algorithm for CT. *IEEE Trans Med Imaging*, 20(10):999–1008, 2001.

[11] Jan Modersitzki and Bernd Fischer. Optimal image registration with a guaranteed one-to-one point match. In Thomas Wittenberg, Peter Hastreiter, Ulrich Hoppe, Heinz Handels, Alexander Horsch, and Hans-Peter Meinzer, editors, *Bildverarbeitung fr die Medizin 2003, Algorithmen - Systeme - Anwendungen*, volume 80, pages 1–5. Technical University of Aachen (RWTH), CEUR Workshop Proceedings, 2003.

[12] OpenDX homepage. `http://www.opendx.org`, 2000.

[13] The HYPRE solver library homepage. `www.llnl.gov/CASC/hypre`, 2004.

[14] J. Bonet and R.D. Wood. *Nonlinear Continuum Mechanics for the Finite Element Analysis*. Cambridge University Press,Cambridge, 1997.

[15] T. Belytschko, W.K. Liu, and B. Moran. *Nonlinear Finite Elements for Continua and Structures*. Wiley & Sons, Chichester, 2000.

[16] Y.C. Fung. *Biomechanics: Mechanical Properties of Living Tissues*. Springer, Berlin, 2 edition, 1993.

[17] J.C. Simo and M.S. Rifai. A Class of Mixed Assumed Strain Methods and the Method of Incompatible Modes. *Int. J. Num. Meth. Engng.*, 29:1595–1638, 1990.

[18] J.C. Simo and F. Armero. Geometrically Non-Linear Enhanced Strain Mixed Methods and the Method of Incompatible Modes. *Int. J. Num. Meth. Engng.*, 33:1413–1449, 1992.

[19] P. Wriggers and J. Korelc. On Enhanced Strain Methods for Small and Finite Deformations of Solids. *Comput. Mech.*, 18:413–428, 1996.

[20] S. Reese, M. Küssner, and B.D. Reddy. A New Stabilization Technique for Finite Elements in Non-Linear Elasticity. *Int. J. Num. Meth. Engng.*, 44:1617–1652, 1999.